NANO LETTERS

Letter

pubs.acs.org/NanoLett

Low-Cost High-Performance Solid-State Asymmetric Supercapacitors Based on MnO_2 Nanowires and Fe_2O_3 Nanotubes

Peihua Yang,[†] Yong Ding,[‡] Ziyin Lin,[‡] Zhongwei Chen,[†] Yuzhi Li,[†] Pengfei Qiang,[†] Masood Ebrahimi,[‡] Wenjie Mai,*[,†,‡] Ching Ping Wong,[‡] and Zhong Lin Wang*[,‡,§]

[†]Department of Physics and Siyuan Laboratory, Jinan University, Guangzhou, Guangdong 510632, China

[‡]School of Materials Science and Engineering, Georgia Institute of Technology, Atlanta, Georgia 30332, United States

[§]Beijing Institute of Nanoenergy and Nanosystems, Chinese Academy of Sciences, Beijing, China

Supporting Information

ABSTRACT: A low-cost high-performance solid-state flexible asymmetric supercapacitor (ASC) with α-MnO_2 nanowires and amorphous Fe_2O_3 nanotubes grown on flexible carbon fabric is first designed and fabricated. The assembled novel flexible ASC device with an extended operating voltage window of 1.6 V exhibits excellent performance such as a high energy density of 0.55 mWh/cm^3 and good rate capability. The ASC devices can find numerous applications as effective power sources, such as powering color-switchable sun glasses and smart windows.

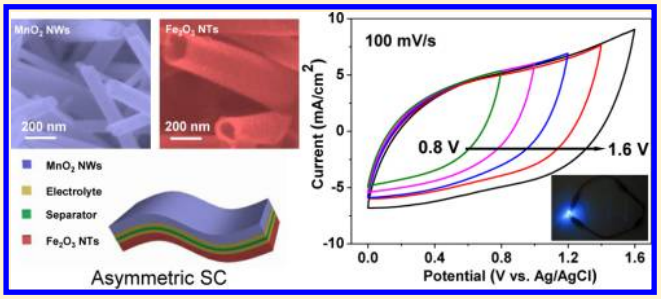

KEYWORDS: *Supercapacitor, asymmetric, flexible, MnO_2, Fe_2O_3*

The large proliferation of consumer electronics generally required high-energy-density and long-lasting power sources. Among the various energy storage technologies, supercapacitors (SCs) have attracted much attention due to their high power density and exceptionally long cycle life.[1,2] However, the energy density (E) is usually limited to the operating voltage (V) according to the equation $E = 1/2CV^2$, where C is the device capacitance. Asymmetric supercapacitors (ASCs) design is an effective approach for extending the operating voltage window and provides effective power sources to meet the demands of emerging technologies.[3,4] Greatly enhanced performance has kindled the interest of researchers in the field of ASCs designs, such as MnO_2//carbon or graphene,[5−7] MnO_2//Fe_3O_4,[8] graphene-RuO_2//graphene,[9] single-walled carbon nanotube (SWCNT)-MnO_2//SWCNT-In_2O_3,[10] CNT-MnO_2//CNT-SnO_2,[11] graphene-$Ni(OH)_2$//graphene,[12] Co_9S_8//Co_3O_4@RuO_2,[13] CoO@polypyrrole//activated carbon,[14] and polyaniline//WO_{3-x}@MoO_{3-x},[15] but most of them still use liquid electrolytes. In comparison to liquid electrolyte SCs, solid-state SCs hold many advantages such as environmental friendliness, portability, flexibility, and stability.[16−19] In this regard, solid-state ASCs have promising applications in durable and flexible electronics. Currently, portable and flexible devices are expected to have a huge market potential and flexible energy storage devices hold the key to realizing portable and flexible electronic devices.

However, solid-state SCs also face some challenges such as low energy density. For instance, SWCNT-based symmetric SC was reported with an energy density of 0.01 mWh/cm^3 and TiN symmetric SC of 0.05 mWh/cm^3.[20,21] Recently, due to potential broader operating voltage windows people have begun to design ASCs with enhanced performance. For example, Lu et al. developed a solid-state flexible ASC device with hydrogenated TiO_2@MnO_2 core−shell nanowires (NWs) as the positive electrode and hydrogenated TiO_2@C core−shell NWs as the negative electrode.[22] Their device operated at 1.8 V and was able to deliver a high specific capacitance of 139.6 F/g and maximum volumetric energy density of 0.30 mWh/cm^3. Despite all these achievements, the facile scalable fabrication of low-cost high-performance solid-state flexible ASCs still remains a challenge.

In the present, transition metal oxides none the less dominate the landscape of active materials for electrochemical energy storage. Manganese dioxide (MnO_2) has significant predominance such as low cost, abundant resource, and high theoretical specific capacitance (1370 F/g).[23,24] Iron oxide (Fe_2O_3) has the advantage of low cost and environmental harmlessness and shows a superior electrochemical performance in negative potential.[25−27] Therefore, ASCs combined with MnO_2 as the positive electrode and Fe_2O_3 as the negative electrode will become a promising energy storage technology that possesses more economical and environmental superiority. It is carbon-based materials that are commonly applied in one of the electrodes in previously reported ASCs (usually worked as negative electrode);[3,22] in this work, however, we focused on enhancing the capacitance and energy density of solid-state flexible ASC based on pseudocapacitance in both electrodes. To the best of our knowledge, this is the first report of a new ASC system based on MnO_2 and Fe_2O_3, two very low-cost metal

Received: October 27, 2013
Revised: December 23, 2013

   dx.doi.org/10.1021/nl404008e | *Nano Lett.* XXXX, XXX, XXX−XXX

oxides synthesized by facile scalable wet chemical methods. The special one-dimensional NW and nanotube (NT) nanoarchitecture can exert the potential electrochemical performance of the active materials due to their high interfacial area and short ion diffusion path. Uniform MnO_2 NWs and Fe_2O_3 NTs were grown directly on a flexible carbon cloth. The conductive carbon cloth not only served as a lightweight and flexible current collector, but also acted as an excellent scaffold for active materials. The high-performance solid-state flexible ASCs fabricated with low-cost MnO_2 NWs (positive electrode) and Fe_2O_3 NTs (negative electrode) achieved a high energy density of 0.55 mWh/cm^3. In addition, the tandem ASCs has been demonstrated to drive a tungsten trioxide (WO_3) based electrochromic device, implying the broad potential applications of these flexible ASCs as power sources.

The growth procedures of NW and NT electrodes are illustrated in Figure 1a and the design of ASC is schematically

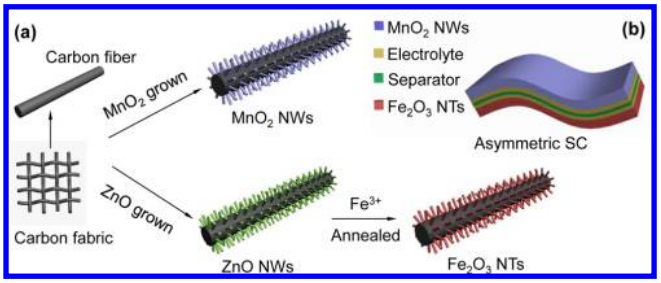

Figure 1. (a) Schematic diagram illustrating the synthesis procedure of MnO_2 NWs and Fe_2O_3 NTs on carbon cloth. (b) Schematic sketch illustrating the designed asymmetric supercapacitor device.

displayed in Figure 1b. Highly ordered MnO_2 NWs were synthesized by a hydrothermal approach.[28] Figure 2a shows SEM images of as-prepared MnO_2 NWs. The carbon fibers were covered by MnO_2 NWs with diameters of 100−150 nm and lengths of 2−4 μm. TEM image (Supporting Information Figure S1a) collected from a typical MnO_2 nanostructure also confirmed the NW morphology, and selected area electron diffraction (SAED) pattern (inset of Figure 2b) of the NW indicated that the NW was single crystal α-MnO_2. The SAED pattern can be indexed as along the beam direction of α-MnO_2 zone axis $[1\bar{1}1]$ (the simulated pattern is provided in Supporting Information Figure S1c for comparison). SAED pattern combined with the shadow image (Supporting Information Figure S1b) suggests that the growth direction of this MnO_2 NW is very close to the normal direction of the $(\bar{1}12)$ plane. The lattice fringe spacing was measured to be ~0.69 nm in high-resolution TEM (HRTEM) image (Figure 2b), corresponding to d-spacing of (110) planes of MnO_2. The energy dispersive X-ray spectrometry (EDS) spectrum in Figure 2c shows the existence of elements Mn, O, K, C, and Cu. Signals of C and Cu come from the TEM copper grid, and the signal of K is found because K ions were introduced to the lattice channels of α-MnO_2 during synthesis.[28] The inductively coupled plasma atomic emission spectroscopy results suggested that the atomic ratio of K to Mn is 0.11:1, very close to the previous reports. As shown in the XRD pattern (Figure 2d), all the diffraction peaks can be indexed to tetragonal α-MnO_2 except the crystalline peak at 25.8° coming from carbon fabric substrate. X-ray photoelectron spectroscopy (XPS) analysis (Supporting Information Figure S3a−c) and electron energy loss spectroscopy (EELS) spectrum (Supporting Information Figure S1d) suggested that the Mn valence is close to +4 in the MnO_2 NWs product by analyzing both Mn 3s and O 1s data (see the Supporting Information).[23,29]

A sacrificial template-accelerated hydrolysis method was used to grow Fe_2O_3 NTs on a carbon fabric.[30] ZnO NWs (Supporting Information Figure S2a) grown on carbon fibers were used as original template and immersed in an aqueous solution containing Fe^{3+} (see the Supporting Information Methods). Figure 3a displays representative SEM image of the well-defined Fe_2O_3 NTs. The columnar NTs uniformly coated on the carbon fibers with outer diameters ranging from 100 to 200 nm. TEM (Supporting Information Figure S2b) image clearly identifies the nanotube structure. As shown Figure 3b, the HRTEM image and SAED pattern both reveal the amorphous structure of these NTs. A typical high-angle annular dark-field (HAADF) scanning transmission electron microscopy (STEM) image of Fe_2O_3 NTs is shown in Figure 3c. EDS spectrum confirmed the existence of elements Fe and O (Figure 3d), and the line scanning spectra (inset of Figure 3d and Supporting Information Figure S2c) of Fe, O, and overall signals across the NT (the line trace is indicated in Figure 3c) can better illustrate the NT configuration. Analysis of the data indicated that the outer and inner diameters of the Fe_2O_3 NT were about 130 and 50 nm, respectively, in accordance with the HAADF STEM image (Figure 3c). XPS analysis (Supporting Information Figure S3d−f) and EELS spectrum (Supporting Information Figure S2d) further confirmed the composition of this NT was Fe_2O_3.[31,32]

The electrochemical studies for the MnO_2 NWs and Fe_2O_3 NTs were conducted in a three-electrode configuration. A piece of NW or NT electrode (effective area ~1 cm^2) was dipped into 5 M LiCl solution at room temperature for a single electrode test. Ag/AgCl reference electrode and graphite rod counter electrode were used in the measurement. Figure 4a,b shows the cyclic voltammetry (CV) curves of MnO_2 positive electrode and Fe_2O_3 negative electrode at different scan rates, respectively. The good reversibility behavior is manifested in the nearly mirror-image current response on voltage reversal in MnO_2 CV curves. A proposed charge storage mechanism of MnO_2 electrodes involved a redox reaction between the III and IV oxidation states of Mn accompanying the cation absorption/desorption or intercalation/deintercalation.[23] It has been found and generally accepted that Mn(III) in the as-prepared manganese oxide will be oxidized to Mn(IV) during charging and subsequently reduced to Mn(III) during discharging. All of the Fe_2O_3 CV curves exhibited a semirectangular shape that was an indicative of pseudocapacitive behavior. The pseudocapacitance of Fe_2O_3 might arise from a reversible Fe^{3+}/Fe^{2+} couple, while the identity of the charge cations involved in the redox reaction was yet undetermined.[33] Typical galvanostatic charge/discharge curves of MnO_2 and Fe_2O_3 electrode collected at different current densities are shown in Supporting Information Figure S4. The areal capacitances and the specific capacitances are calculated from galvanostatic charge/discharge curves and shown in Figure 4c. The areal capacitance of the MnO_2 and Fe_2O_3 electrode achieved 150.0 and 180.4 mF/cm^2 at a current density of 1 mA/cm^2. The specific capacitance corresponded to 197.4 and 257.8 F/g (at an equivalent current density of 1.3 A/g and 1.4 A/g, respectively). The capacitance of MnO_2 was much better than the values reported for other manganese oxide composites (111 F/g at 1.8 A/g for 45 min carbon nanoparticles/MnO_2 nanorods[34] and 170 F/g at 1 A/g for 5 min activated microwave-expanded graphite oxide/MnO_2 composite[35]); meanwhile, the performance of Fe_2O_3 was better than the previous reported (138 F/g at 1.3 A/g[36] and 173 F/g at 3 A/g[37]). Even at a high current density of 10 mA/cm^2, the areal capacitance of the MnO_2 and Fe_2O_3 electrode retained at 110.4 and

dx.doi.org/10.1021/nl404008e | Nano Lett. XXXX, XXX, XXX−XXX

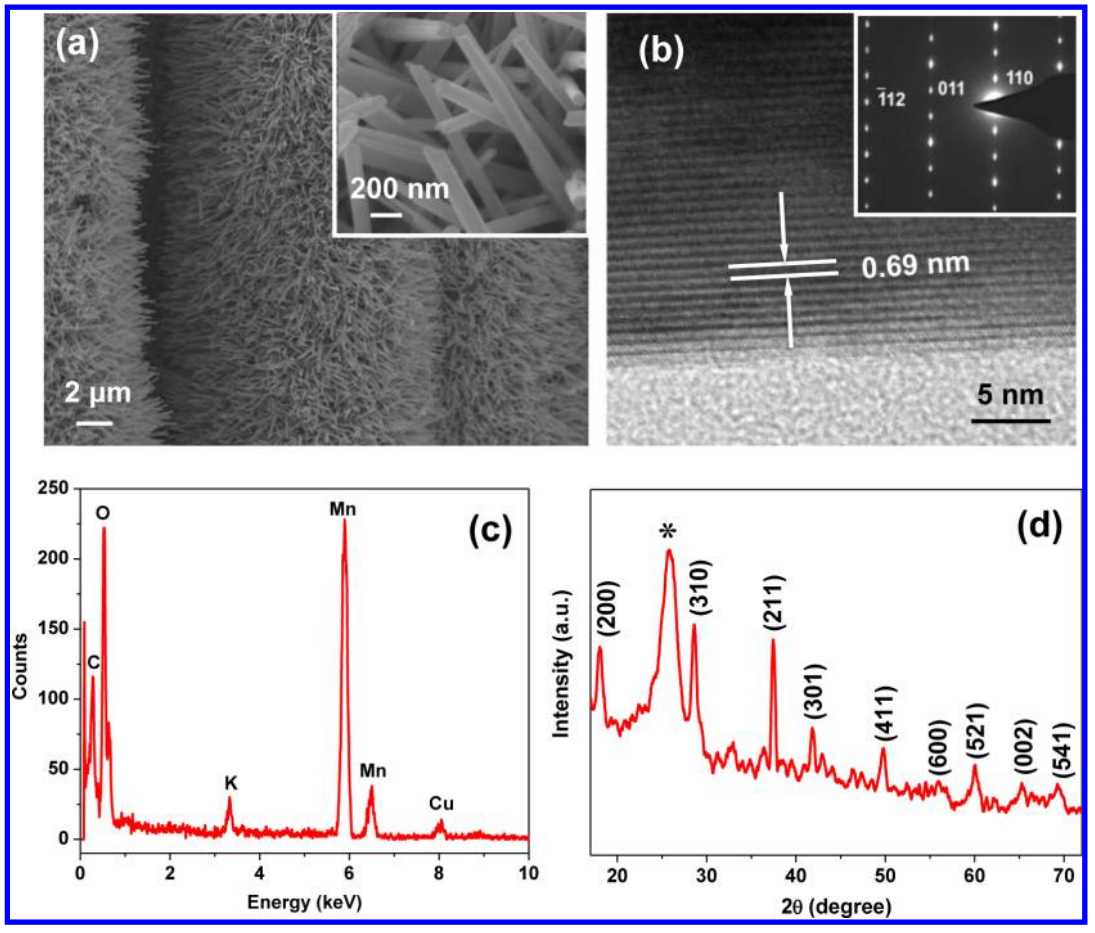

Figure 2. (a) SEM image of MnO_2 NWs (inset is magnified SEM image). (b) HRTEM image of MnO_2 NWs (inset is SAED pattern). (c) EDS spectrum of MnO_2 NWs. (d) XRD pattern suggesting α-MnO_2. Peak * represents the characteristic peak of carbon fabric substrate.

119.9 mF/cm^2, showing good rate capacitance of 73.6 and 66.5%, respectively. The outstanding rate capability could be attributed to the remarkable conductivity of the carbon fabric substrate. According to the electrochemical impedance spectroscopy (EIS) curves in Figure 4d, the equivalent series resistance (ESR) of MnO_2 and Fe_2O_3 electrode was only 3.99 and 4.32 Ω cm^2, which suggested good conductivity for both positive and negative electrode, benefiting from the excellent conductivity of carbon cloth substrate. Although the conductivity of Fe_2O_3 is better that of MnO_2, probably due to the different loading mass and dimensions, the ESR value of Fe_2O_3 is slightly larger than that of MnO_2.

A solid-state flexible asymmetric SC was assembled with MnO_2 NWs and Fe_2O_3 NTs electrodes using a gel electrolyte (Figure 1b). According to the CV studies for single electrode, an operating cell voltage from 0.8 to 1.6 V was applied to the ASCs. Figure 5a demonstrates the CV curves collected at 100 mV/s in different voltage windows for the MnO_2//Fe_2O_3 solid-state flexible ASC. The fabricated ASC showed a typical capacitive behavior with nearly rectangular CV curves. The flexible ASC demonstrates good performance behavior under different testing conditions (Supporting Information Figure S6), revealing good flexibility and stability. Galvanostatic charge/discharge curves of different current density are shown in Figure 5b. Discharge curves were almost symmetrical to the corresponding charge curves, indicating good capacitive behavior for the ASC device. Figure 5c demonstrates the calculated specific capacitance and volumetric capacitance based on the discharge curves. The solid-state flexible ASC device achieved a high specific and volumetric capacitance of 91.3 F/g and 1.5 F/cm^3 at a current density of 2 mA/cm^2, which was much higher than recent reports for other solid-state ASCs, such as RGO-MnO_2//RGO paper (22.7 F/g at 0.05 mA/cm^2)[38] and VO_x//VN (52 F/g at 2 mA/cm^2).[39] Furthermore, the solid-state flexible ASC device showed good rate performance with 58.6% of volumetric capacitance retained when the current density increased from 2 to 10 mA/cm^2, which could be ascribed to the unique nanostructure with large surface area and high electrical conductivity of carbon fabric. Abundant adsorption of ions as well as efficient ion intercalation/deintercalation and charge transport promoted the good rate capability.

Energy density and average power density are two important parameters for the SC device. Figure 5d shows the Ragone plot of our ASC device. The solid-state ASC exhibited a high energy density of 0.55 mWh/cm^3, which even can be comparable to the latest report for VO_x//VN ASC (0.61 mWh/cm^3).[39] Moreover, high power density of 139.1 mW/cm^3 was obtained while the energy density was still as high as 0.32 mWh/cm^3 at discharge current density of 10 mA/cm^2. A simple application to light a commercial blue light-emitting diode (LED) was demonstrated. The tandem ASCs (two devices connected in series) could easily light up a blue LED after being charged to 3.2 V (Figure 5d inset). The cycle life of the ASC was tested through a cyclic charge/discharge process at a current density of 2 mA/cm^2 in different operating voltage window for 6000 cycles (Figure 5e). Although the capacitance retention had obvious fluctuation when the

dx.doi.org/10.1021/nl404008e | Nano Lett. XXXX, XXX, XXX−XXX

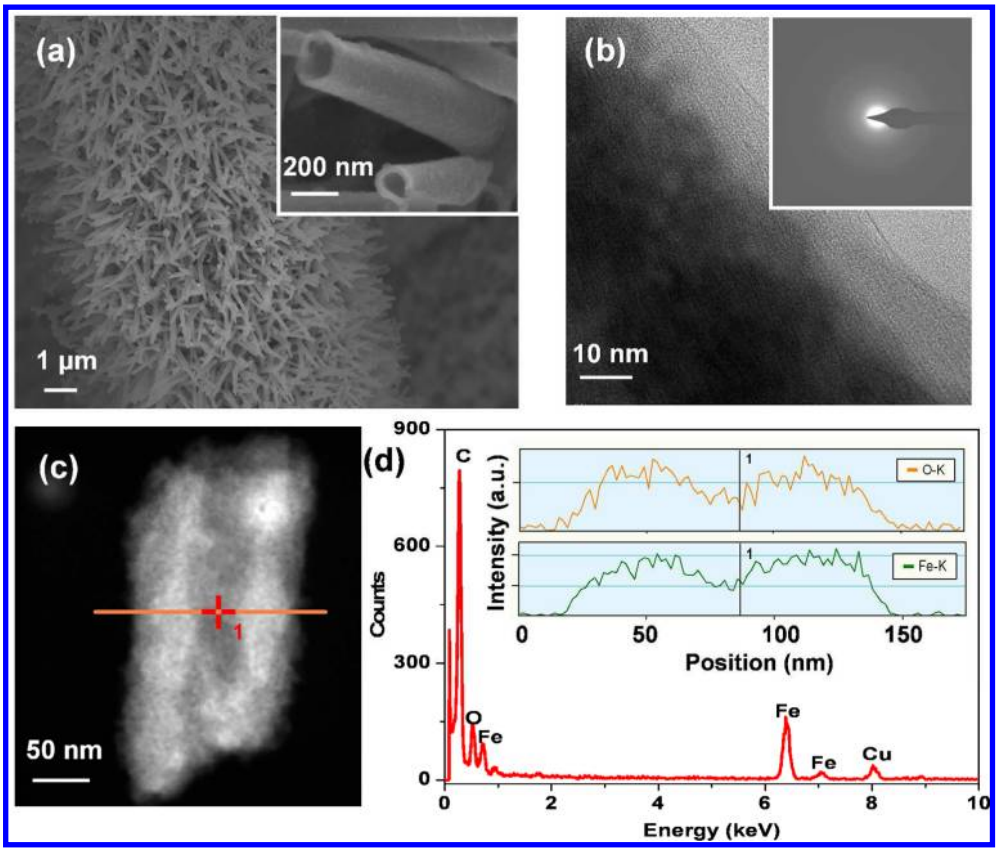

Figure 3. (a) SEM image of Fe_2O_3 NTs (inset is magnified SEM image). (b) HRTEM image of Fe_2O_3 NTs (inset is SAED pattern) suggesting amorphous phase. (c) HAADF STEM image of Fe_2O_3 NTs. (d) EDS spectrum of the Fe_2O_3 NTs. The insets are EDS line scan curves showing Fe and O element distribution across the Fe_2O_3 NTs indicated by a line in (c).

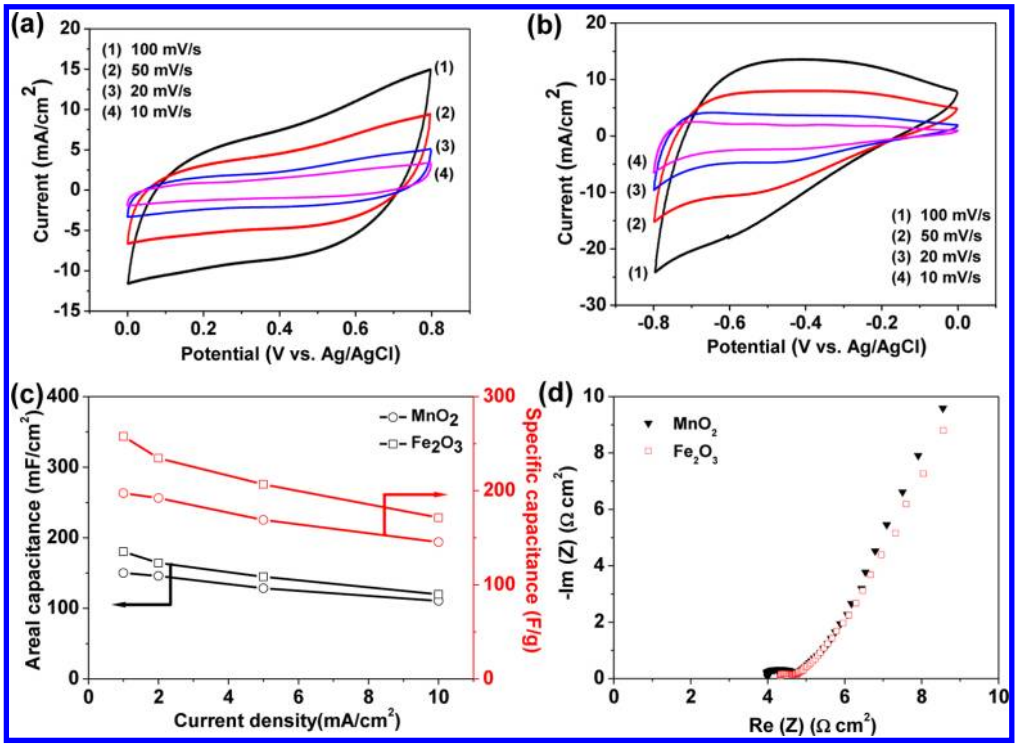

Figure 4. CV curves for (a) MnO_2 NWs and (b) Fe_2O_3 NTs collected at different scan rates. (c) Areal and specific capacitance calculated from the charge/discharge curves as a function of current density. (d) Nyquist plots of MnO_2 NWs and Fe_2O_3 NTs electrodes with an area of 1 cm^2.

potential window changed, the solid-state ASC device still exhibited 84% retention of the initial capacitance after 5000 cycles. That excellent stability might be due to the solid electrolyte, suppressing the dissolution of MnO_2 and Fe_2O_3. To conjecture

dx.doi.org/10.1021/nl404008e | *Nano Lett.* XXXX, XXX, XXX−XXX

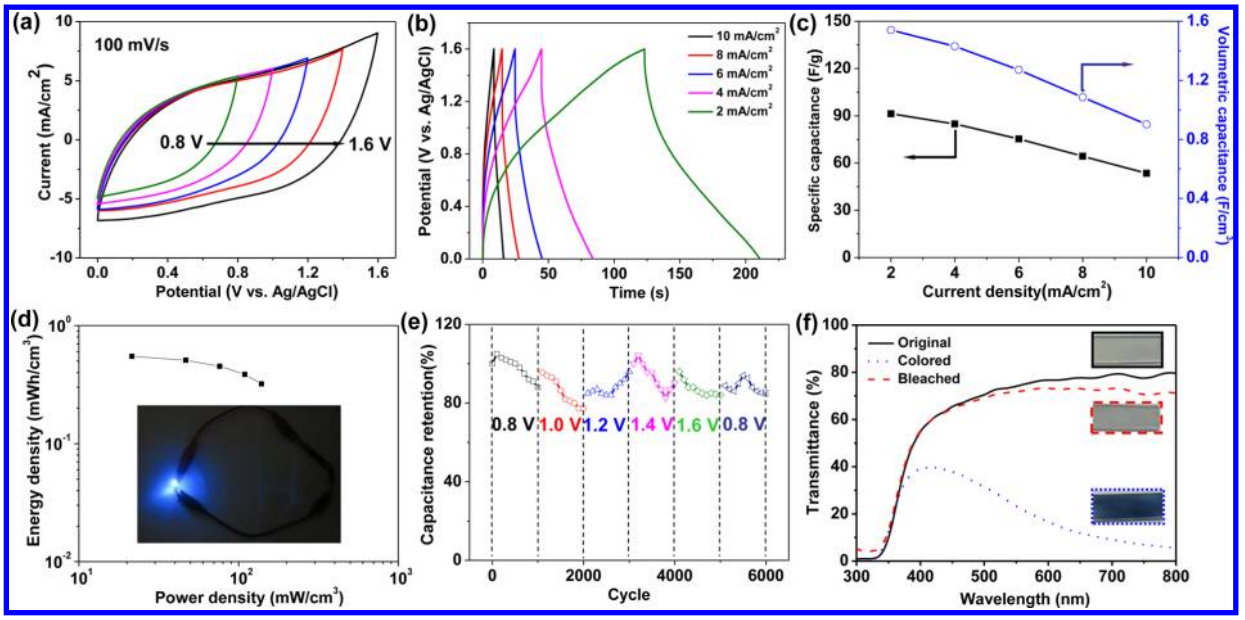

Figure 5. (a) CV curves of the assembled solid-state ASC device collected in different scan voltage windows. (b) Galvanostatic charge/discharge curves of ASC device collected at different current density. (c) Specific and volumetric capacitance calculated from the charge/discharge curves as a function of current density. (d) Ragone plots of the solid-state ASC device. Inset shows a blue LED powered by the tandem ASC devices. (e) Cycle performance the ASC device measured at a current density of 2 mA/cm^2 under various potential windows. (f) Transmittance spectra of the WO_3 electrode in original, colored, and bleached states. Insets are the corresponding photos of the same WO_3 electrode under the different conditions.

the degradation of the capacitance, EIS test was conducted. The ESR of the device increased from 3.9 to 7.4 Ω cm^2 after 5000 cycles charge/discharge process (Supporting Information Figure S7). The distortion of charge transport pathway during the long-term cycles might result in the increase of ESR, which was caused by a combined effect of the degradation of the electrolyte, separator, and even the active materials.[40]

The reversible electrochromic change in transparency has promising applications in smart windows and portable displays.[41,42] WO_3 is an effective electrochromic material and has been widely studied. Herein, we built an electrochromic system consisting of tandem ASCs and a homemade WO_3 smart glass (Supporting Information Figure S8). The WO_3 film was directly grown on an FTO glass. SEM and atomic force microscopy images (Supporting Information Figure S9) indicate the film is composed of uniform grain with average grain size of 306 nm and average roughness parameters R_q of 34 nm and R_a of 27 nm.

In a typical electrochromic process, the tandem ASCs were first charged to 3 V and then connected them with the WO_3 glass electrode and the Pt reference electrode using 1 M H_2SO_4 electrolyte. Strikingly, the transparency of the electrode decreased from 79.6 to 5.6% in 5 s after tandem ASCs were connected and backed to 71.2% in 4 s after the polarity of the ASCs was reversely connected. The transmittance spectra are recorded the Figure 5f. The results demonstrate the feasibility that our solid-state ASCs could act as voltage power sources for electrochromic systems. The further integration and miniaturization of ASCs and electrochromic device as stand-alone color-switchable sun glasses and smart windows can find broad applications in energy conservation, environmental protection, and everyday life. As previous literatures reported, SCs can be integrated and charged with other stand-alone power sources such as dye-sensitized solar cells and nanogenerators,[43−47] composing an even more promising self-power system.

In summary, a durable solid-state flexible ASC based on low-cost MnO_2 NWs and Fe_2O_3 NTs was first designed and fabricated via a facile scalable method. Comparing with previously reported solid state SCs, our newly desgined ASCs demonstrated excellent stability in a large potential window of 1.6 V and exhibited excellent energy density of 0.55 mWh/cm^3. Additionally, our ASC showed good flexibility and high rate capability. Moreover, an application of our high-performance ASCs in effectively switching colors of electrochromic systems was demonstrated, promoting our low-cost high-performance solid-state ASCs to be a highly promising candidate for next-generation energy storage systems.

■ ASSOCIATED CONTENT

Ⓢ Supporting Information

Synthetic and characterization methods, calculation methods, SEM, TEM, and EELS images, XPS spectra, CV and charge/discharge curves, EIS spectra, and electrochromic system. This material is available free of charge via the Internet at http://pubs.acs.org.

■ AUTHOR INFORMATION

Corresponding Authors

*E-mail: wenjiemai@gmail.com (W.J.M.).
*E-mail: zlwang@gatech.edu (Z.L.W.).

Notes

The authors declare no competing financial interest.

■ ACKNOWLEDGMENTS

P.H.Y acknowledges the financial support from the Jinan University Outstanding Student Program. W.J.M. thanks the National Natural Science Foundation of China (Grants 51102115 and 21376104), the Natural Science Foundation of Guangdong Province, China (Grant S2013010012876), and the China Scholarship Council (Grant 201206785006) for financial support. Z.L.W. thanks the Knowledge Innovation Program of the Chinese Academy of Sciences (KJCX2-YW-M13) for financial support. The authors thank Mr. X. Xiao and Professor J. Zhou from the

Huazhong University of Science and Technology for helpful discussions and experiment assistance.

REFERENCES

(1) Conway, B. E. *Electrochemical Supercapacitor: Scientific Fundamentals and Technological Applications*; Kluwer Academic/Plenum: New York, 1999.
(2) Simon, P.; Gogotsi, Y. *Nat. Mater.* **2008**, *7*, 845.
(3) Long, J. W.; Bélanger, D.; Brousse, T.; Sugimoto, W.; Sassin, M. B.; Crosnier, O. *MRS Bull.* **2011**, *36*, 513.
(4) Chae, J. H.; Ng, K. C.; Chen, G. Z. *Proc. Inst. Mech. Eng., Part A* **2010**, *224*, 479.
(5) Khomenko, V.; Raymundo-Piñero, E.; Béguin, F. *J. Power Sources* **2006**, *153*, 183.
(6) Wu, Z.-S.; Ren, W.; Wang, D.-W.; Li, F.; Liu, B.; Cheng, H.-M. *ACS Nano* **2010**, *4*, 5835.
(7) Lei, Z.; Zhang, J.; Zhao, X. S. *J. Mater. Chem.* **2012**, *22*, 153.
(8) Brousse, T.; Belanger, D. *Electrochem. Solid-State Lett.* **2003**, *6*, A244.
(9) Choi, B. G.; Chang, S.-J.; Kang, H.-W.; Park, C. P.; Kim, H. J.; Hong, W. H.; Lee, S.; Huh, Y. S. *Nanoscale* **2012**, *4*, 4983.
(10) Chen, P.-C.; Shen, G.; Shi, Y.; Chen, H.; Zhou, C. *ACS Nano* **2010**, *4*, 4403.
(11) Ng, K. C.; Zhang, S.; Peng, C.; Chen, G. Z. *J. Electrochem. Soc.* **2009**, *156*, A846.
(12) Yan, J.; Fan, Z.; Sun, W.; Ning, G.; Wei, T.; Zhang, Q.; Zhang, R.; Zhi, L.; Wei, F. *Adv. Funct. Mater.* **2012**, *22*, 2632.
(13) Xu, J.; Wang, Q.; Wang, X.; Xiang, Q.; Liang, B.; Chen, D.; Shen, G. *ACS Nano* **2013**, *7*, 5453.
(14) Zhou, C.; Zhang, Y.; Li, Y.; Liu, J. *Nano Lett.* **2013**, *13*, 2078.
(15) Xiao, X.; Ding, T.; Yuan, L.; Shen, Y.; Zhong, Q.; Zhang, X.; Cao, Y.; Hu, B.; Zhai, T.; Gong, L.; Chen, J.; Tong, Y.; Zhou, J.; Wang, Z. L. *Adv. Energy Mater.* **2012**, *2*, 1328.
(16) Xiao, X.; Li, T.; Yang, P.; Gao, Y.; Jin, H.; Ni, W.; Zhan, W.; Zhang, X.; Cao, Y.; Zhong, J.; Gong, L.; Yen, W.-C.; Mai, W.; Chen, J.; Huo, K.; Chueh, Y.-L.; Wang, Z. L.; Zhou, J. *ACS Nano* **2012**, *6*, 9200.
(17) Lu, X.; Zhai, T.; Zhang, X.; Shen, Y.; Yuan, L.; Hu, B.; Gong, L.; Chen, J.; Gao, Y.; Zhou, J.; Tong, Y.; Wang, Z. L. *Adv. Mater.* **2012**, *24*, 938.
(18) Yuan, L.; Yao, B.; Hu, B.; Huo, K.; Chen, W.; Zhou, J. *Energy Environ. Sci.* **2013**, *6*, 470.
(19) El-Kady, M. F.; Strong, V.; Dubin, S.; Kaner, R. B. *Science* **2012**, *335*, 1326.
(20) Kaempgen, M.; Chan, C. K.; Ma, J.; Cui, Y.; Gruner, G. *Nano Lett.* **2009**, *9*, 1872.
(21) Lu, X.; Wang, G.; Zhai, T.; Yu, M.; Xie, S.; Ling, Y.; Liang, C.; Tong, Y.; Li, Y. *Nano Lett.* **2012**, *12*, 5376.
(22) Lu, X.; Yu, M.; Wang, G.; Zhai, T.; Xie, S.; Ling, Y.; Tong, Y.; Li, Y. *Adv. Mater.* **2013**, *25*, 267.
(23) Toupin, M.; Brousse, T.; Bélanger, D. *Chem. Mater.* **2004**, *16*, 3184.
(24) Lang, X.; Hirata, A.; Fujita, T.; Chen, M. *Nat. Nanotechnol.* **2011**, *6*, 232.
(25) Qu, Q.; Yang, S.; Feng, X. *Adv. Mater.* **2011**, *23*, 5574.
(26) Wu, M. S.; Ou, Y. H.; Lin, Y. P. *Electrochim. Acta* **2010**, *55*, 3240.
(27) Wu, M.-S.; Lee, R.-H. *J. Electrochem. Soc.* **2009**, *156*, A737.
(28) Luo, J.; Zhu, H. T.; Fan, H. M.; Liang, J. K.; Shi, H. L.; Rao, G. H.; Li, J. B.; Du, Z. M.; Shen, Z. X. *J. Phys. Chem. C* **2008**, *112*, 12594.
(29) Chigane, M.; Ishikawa, M. *J. Electrochem. Soc.* **2000**, *147*, 2246.
(30) Liu, J.; Li, Y.; Fan, H.; Zhu, Z.; Jiang, J.; Ding, R.; Hu, Y.; Huang, X. *Chem. Mater.* **2010**, *22*, 212.
(31) Yamashita, T.; Hayes, P. *Appl. Surf. Sci.* **2008**, *254*, 2441.
(32) Asami, K.; Hashimoto, K. *Corros. Sci.* **1977**, *17*, 559.
(33) Sassin, M. B.; Mansour, A. N.; Pettigrew, K. A.; Rolison, D. R.; Long, J. W. *ACS Nano* **2010**, *4*, 4505.
(34) Yuan, L.; Lu, X.-H.; Xiao, X.; Zhai, T.; Dai, J.; Zhang, F.; Hu, B.; Wang, X.; Gong, L.; Chen, J.; Hu, C.; Tong, Y.; Zhou, J.; Wang, Z. L. *ACS Nano* **2012**, *6*, 656.
(35) Zhao, X.; Zhang, L.; Murali, S.; Stoller, M. D.; Zhang, Q.; Zhu, Y.; Ruoff, R. S. *ACS Nano* **2012**, *6*, 5404.
(36) Xie, K.; Li, J.; Lai, Y.; Lu, W.; Zhang, Z. a.; Liu, Y.; Zhou, L.; Huang, H. *Electrochem. Commun.* **2011**, *13*, 657.
(37) Wu, M.-S.; Lee, R.-H.; Jow, J.-J.; Yang, W.-D.; Hsieh, C.-Y.; Weng, B.-J. *Electrochem. Solid-State Lett.* **2009**, *12*, A1.
(38) Sumboja, A.; Foo, C. Y.; Wang, X.; Lee, P. S. *Adv. Mater.* **2013**, *25*, 2809.
(39) Lu, X.; Yu, M.; Zhai, T.; Wang, G.; Xie, S.; Liu, T.; Liang, C.; Tong, Y.; Li, Y. *Nano Lett.* **2013**, *13*, 2628.
(40) Wang, W.; Guo, S.; Penchev, M.; Ruiz, I.; Bozhilov, K. N.; Yan, D.; Ozkan, M.; Ozkan, C. S. *Nano Energy* **2012**, *2*, 294.
(41) Yang, X.; Zhu, G.; Wang, S.; Zhang, R.; Lin, L.; Wu, W.; Wang, Z. L. *Energy Environ. Sci.* **2012**, *5*, 9462.
(42) Wei, Z.; Wang, K.; Wu, H.; Meng, Y.; Zhang, Y. *Energy Environ. Sci.* **2012**, *5*, 8384.
(43) Yang, P.; Xiao, X.; Li, Y.; Ding, Y.; Qiang, P.; Tan, X.; Mai, W.; Lin, Z.; Wu, W.; Li, T.; Jin, H.; Liu, P.; Zhou, J.; Wong, C. P.; Wang, Z. L. *ACS Nano* **2013**, *7*, 2617.
(44) Pan, C.; Guo, W.; Dong, L.; Zhu, G.; Wang, Z. L. *Adv. Mater.* **2012**, *24*, 3356.
(45) Chen, T.; Qiu, L.; Yang, Z.; Cai, Z.; Ren, J.; Li, H.; Lin, H.; Sun, X.; Peng, H. *Angew. Chem., Int. Ed.* **2012**, *51*, 11977.
(46) Yuan, L.; Xiao, X.; Ding, T.; Zhong, J.; Zhang, X.; Shen, Y.; Hu, B.; Huang, Y.; Zhou, J.; Wang, Z. L. *Angew. Chem., Int. Ed.* **2012**, *51*, 4934.
(47) Hu, Y.; Zhang, Y.; Xu, C.; Lin, L.; Snyder, R. L.; Wang, Z. L. *Nano Lett.* **2011**, *11*, 2572.

dx.doi.org/10.1021/nl404008e | *Nano Lett.* XXXX, XXX, XXX−XXX